# Finite Element Modeling of Micromachined MEMS Photon Devices

B.M. Evans III[*][a], D.W. Schonberger[b], and P.G. Datskos[a,c]

[a]Oak Ridge National Laboratory, MS 8039, Oak Ridge, TN 37830
[b]University of Kansas, Department of Electrical Engineering and Computer Science,
Lawrence, Kansas, 66045
[c]University of Tennessee, Department of Physics, Knoxville, TN, 37996-1200

## ABSTRACT

The technology of microelectronics that has evolved over the past half century is one of great power and sophistication and can now be extended to many applications (MEMS and MOEMS) other than electronics. An interesting application of MEMS quantum devices is the detection of electromagnetic radiation. The operation principle of MEMS quantum devices is based on the photoinduced stress in semiconductors, and the photon detection results from the measurement of the photoinduced bending. These devices can be described as micromechanical photon detectors. In this work, we have developed a technique for simulating electronic stresses using finite element analysis. We have used our technique to model the response of micromechanical photon devices to external stimuli and compared these results with experimental data. Material properties, geometry, and bimaterial design play an important role in the performance of micromechanical photon detectors. We have modeled these effects using finite element analysis and included the effects of bimaterial thickness coating, effective length of the device, width, and thickness.

**Keywords:** Quantum MEMS, photoinduced stress, photostriction, quantum detector, finite element analysis

## 1. INTRODUCTION

Sensing elements are devices that respond to one form of energy and provide an output, which is often in a different form of energy. Detectors are instruments that provide a measurement of the amount of energy absorbed. Several different types of solid state and micromechanical photo-detectors are currently available or are under development.[1] Photo-detectors[2,3] can be categorized as either quantum[4] (photon) detectors or thermal detectors. Quantum detectors include charge-coupled devices (CCDs) and solid state detectors, and they function based on the properties of semiconductors. Thermal detectors convert radiated optical energy into thermal energy and result in an increase in temperature of the detector that can then be measured by various means. Several types of thermal detectors exist including pyroelectric,[5] thermoelectric,[6] resistive micro-bolometers,[7] and microcantilever thermal detectors.[8]

In order to develop techniques for increasing the response and detection threshold for infrared detectors, we have been investigating a new type of micromechanical photon detector.[9,10,11] These semiconductor devices respond based on the internal, electronic stress resulting from the generation of electron-hole pairs. These highly sensitive photon detectors have extensive applications for infrared imaging, spectroscopy,[12] chemical sensing,[13] and energy detection.[9,10,11]
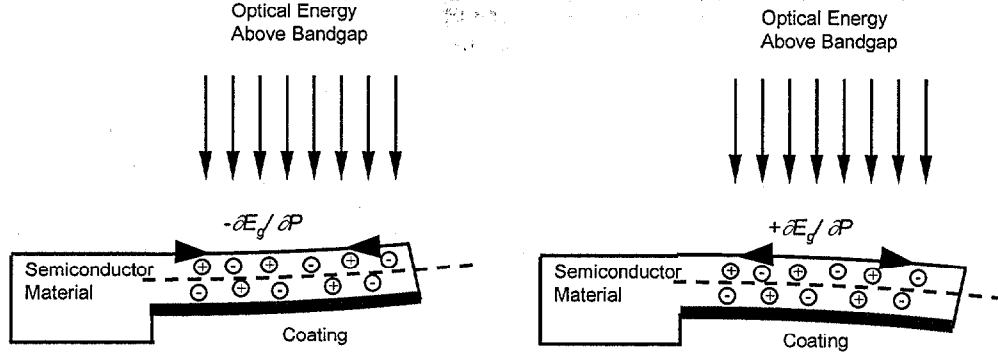
In this research, a new technique for predicting the mechanical response of micro-devices to photoinduced stresses is employed. A simple verification model is solved to determine the accuracy of this method. The numerical technique is also applied to a more complicated microstructure. The results of numerical analysis are compared with experimental data.

### 1.1 Photoinduced Stress

Much research has been performed on the acoustic emission of semiconductor materials through optical excitation.[14,15] The theory of photoinduced stress was reported in 1961 by Figielski,[16] who calculated the change in the lattice constant when excess charge carriers are generated in a semiconductor due to optical illumination. Figielski used a model of the band structure versus interatomic distances to compute the dilation of the crystal lattice and assumed that the elastic properties were related to the valence electrons only. Figielski's formula for the "photostriction" of semiconductors is given by Equation 1, where $\varepsilon_{pi}$ represents photoinduced strain, $n$ is the number of charge carriers, $K$ is the bulk modulus, $(\partial E_g/\partial P)_T$.

---

[*]Correspondence: Email: evansbmiii@ornl.gov; Telephone: 423-574-9418, Fax 423-574-9407

**Figure 1:** Photoinduced bending of semiconductor material with positive and negative bandgap dependence on pressure, $\partial E_g/\partial P$.

represents the bandgap dependence on pressure at a constant temperature, and $c_{11}$ and $c_{12}$ represent the directional moduli of elasticity.

$$\varepsilon_{pi} = \frac{nK\left(\dfrac{\partial E_g}{\partial P}\right)_T}{(c_{11} + 2c_{12})} \tag{1}$$

Equation 1 can be simplified using the definition of bulk modulus,[17] by assuming that Poisson's ratio equals 1/3, and assuming that $c_{11} + 2c_{12}$ is approximately equal to three times Young's modulus, $Y$. We also assume that there is a negligible temperature change in the detector, and therefore the partial derivatives can be represented as general derivatives. This gives the more commonly employed version of the equation for photoinduced strain, which is a linear function of the pressure dependence of bandgap energy and the number of charge carriers created as shown below in Equation 2.[18,14]

$$\varepsilon_{pi} = \frac{1}{3}\left(\frac{dE_g}{dP}\right)\Delta n \tag{2}$$

When photon energy is absorbed by a semiconductor material with bandgap energy, $E_g$, the total change in surface stress, $\Delta s$, is equal to the combination of photoinduced stress, $\Delta s_{pi}$, and the thermal stress, $\Delta s_{th}$, due to temperature change, $\Delta T$. This relationship is shown in Equation 3.[10]

$$\Delta s = \Delta s_{pi} + \Delta s_{th} = \frac{1}{3}\left(\frac{dE_g}{dP}\right)\Delta nY + \alpha\Delta TY = \left(\frac{1}{3}\frac{dE_g}{dP}\Delta n\right)Y + \alpha\Delta TY, \tag{3}$$

where $Y$ refers to the Young's modulus, and $\alpha$ is the linear coefficient of thermal expansion.

Stearns, Kino[14] and others[10] have performed experiments to verify the existence of electronically induced strain in silicon using the property of the negative $dE_g/dP$ in silicon to separate the effects of thermal strains from electronic strain. Figure 1 illustrates this effect.

The linear strain produced with the creation of electron hole pairs can be converted into a bending effect by coating one side of the microcantilever. This bending effect occurs because the two layer experience different amounts of stress based on their modulus of elasticity, thermal expansion coeficients, or differences in $dE_g/dP$ for photoinduced stress. The maximum z deflection, $z_{max}$, for a rectangular beam rigidly attached at one end is given by the following equation:[19,20]

$$z_{max} = \frac{l^2}{t_1 + t_2} \left( \frac{1 + (t_1/t_2)^2}{3(1 + t_1/t_2)^2 + (1 + t_1 Y_1/t_2 Y_2)(t_1^2/t_2^2 + t_2 Y_2/t_1 Y_1)} \right) \frac{Y_1}{Y^*} \frac{\partial E_g}{\partial P} \Delta n, \tag{4}$$

where $t_1$ and $t_2$ are the top and bottom layer thickness, and $Y_1$ and $Y_2$ are the moduli of elasticity for top and bottom layers. $Y^*$ is the effective modulus of elasticity of the coated cantilever given by the equation, $Y^* = Y_1 Y_2/(Y_1 + Y_2)$.

It is assumed in this work that the absorption of photons with energies above the bandgap creates a near instantaneous, isotropic strain in the semiconductor material, and that the distribution of charge carriers is uniform throughout the substrate. The change in charge carrier density, $\Delta n$, in the material can be calculated knowing the quantum efficiency, $\eta$, the charge carrier lifetime, $\tau_L$, the incident wavelength, $\lambda$, Planck's constant, $h$, the speed of light, $c$, the volume of the substrate, $V$, and the total flux absorbed, $\Phi_{abs}$, by Equation 5.[9]

$$\Delta n = \eta \frac{\lambda}{hc} \frac{\tau_L}{V} \Phi_{abs} \tag{5}$$

By examining Equations 4 and 5, it is apparent that the sensitivity of the micromechanical photon detector can be increased by choosing a material with an optimum $dE_g/dP$. In addition, it is possible to improve the sensitivity of the detector by optimizing the charge carrier density, $\Delta n$. The charge carrier density can be increased by several means including reducing the volume of the device by reducing the thickness, using materials that have band gap cutoffs at the longest wavelengths, and by choosing materials with long charge carrier lifetimes or using methods of increasing the charge carrier lifetime, $\tau_L$.

### 1.2 Finite Element Analysis

The concept of structural finite element analysis involves obtaining an approximate solution for the displacement values of a continuum by dividing that continuum into a number of 'finite elements' and solving the function representing the displacement of those nodal points. These elements are connected at a specific number of nodal points on their boundary. Functions are chosen to represent the displacement within the finite element based on the nodal displacements. The displacement functions can be used to determine the state of strain within the finite element as a function of the nodal displacements. The knowledge of these strains combined with any existing internal strains and the elastic properties can be used to determine the state of stress within the elements. Existing internal strains would be the result of thermal expansion, photoinduced strain, or other similar phenomena. A system of forces is applied at the nodal points, which is equal to any distributed loads or applied boundary stresses such that the system is in equilibrium. The element displacement in terms of the applied and internal forces is given by the following equation:

$$\{F\}_a = [k]_a \{\delta\}_a + \{F\}_{a,p} + \{F\}_{a,\varepsilon o} \tag{6}$$

where $\{F\}_a$ is the matrix representing the force vectors at all of the nodes of an element 'a', $\{F\}_{a,p}$ is the force matrix resulting from applied nodal forces or distributed loads, and $\{F\}_{a,\varepsilon o}$ represents forces on the nodes resulting from internal strains, such as thermal or photoinduced strain. The matrix, $[k]_a$, is the element stiffness matrix, and $\{\delta\}_a$ represents the displacements.[21]

It is important to note that like other methods of engineering computation, finite element analysis is a method based on the energy of the system. Often in structural analysis, the system is treated as an array of springs or elastic elements. The energy required to displace the nodes, or strain energy is used to compute the potential energy of the system. One method of obtaining a solution to the large number of matrix equations generated by finite element analysis involves Euler's *Principal of Minimum Total Potential Energy*, also known as the principal of virtual work. On this basis, the finite element equations are solved for the displacement field based on the internal strains, external displacements, and the minimum potential energy. The state of minimum potential energy corresponds to the state of equilibrium.[22,23]
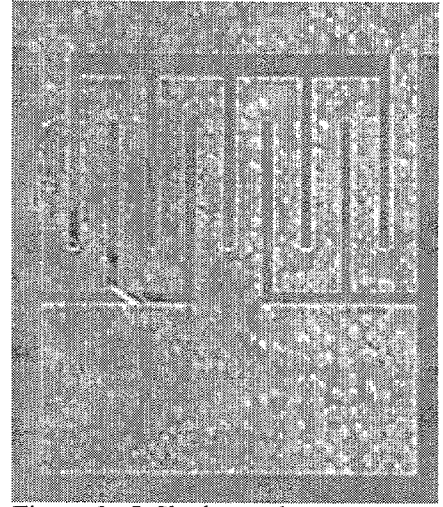
# 2. MICROMECHANICAL PHOTON DETECTOR

For this experiment, a novel micromechanical detector was fabricated using a combination of single point diamond, chemical etching, broad beam ion milling, and focused ion milling. Single point diamond turning was used to fabricate a 50 µm thick diaphragm in an indium antimonide, InSb, substrate. The thickness of the diaphragm was further reduced using a combination of chemical etching and broad beam ion milling. The final structure was fabricated using a focused ion beam to cut out the geometry seen in Figure 2. This was a rectangular shaped photon detector measuring 66µm long by 60µm wide. The legs of the structure were folded five times to minimize the rate at which energy was transferred to the base of the device.
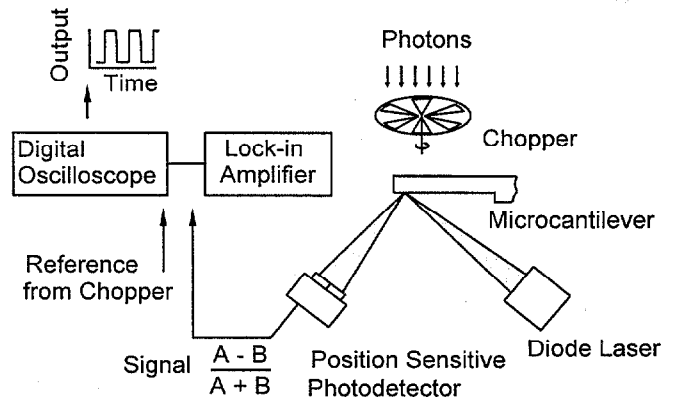
InSb was chosen for this experiment due to its high band gap dependence on pressure, $dE_g/dP$, and for its low bandgap energy. The band gap dependence on pressure for InSb is $+2.45 \times 10^{-23}$ cm$^3$ as compared to silicon, which has a $dE_g/dP$ of $-3.26 \times 10^{-24}$ cm$^3$.[24] InSb is activated by longer wavelength photons (up to 7.5 µm compared to 1 µm for silicon), because InSb has a lower bandgap energy (0.17eV) than Si (1.1eV).[25] The combination of high bandgap dependence on pressure and low bandgap energy means that InSb devices should have an order of magnitude better response than silicon devices.



**Figure 2:** InSb photon detector fabricated using single point diamond turning and focused ion milling.

The InSb micromechanical photon detector was coated with a thin layer (50 nm) of gold, Au. This served two purposes. One purpose was to reflect the readout laser beam. A more important purpose was that the layer helped form a bimaterial structure, which can exhibit bending due to differential expansion of InSb and Au. After coating, the device was heated to 500 C. The heating process helped reduce any residual mechanical stresses that were created as a result of the deposition process. This procedure seemed to result in a microcantilever structure with almost no residual bending in the steady state. However, it is interesting to note that we observed that the resonance frequency of the InSb microstructure was lower than the resonance frequency of the uncoated InSb. It is difficult to say how much of the observed frequency shift was due to pure mass loading, and how much was due to residual stresses.

We investigated the response of our devices using the experimental setup shown in Figure 3. To detect movement of the cantilever, a diode laser (delivering 1 mW at 670 nm) was focused on the tip of the microcantilever using a 20-power microscope objective. In order to minimize heating of the tip by the probe laser, optical power was reduced by placing a neutral density filter with an optical density of 1.0 between the probe laser and the objective. A quad-element (A,B,C,D) photodiode detector was used to collect the reflected probe beam. The current output ($i_{A,B,C,D}$) of the photodiode depends linearly on the bending of the microcantilever. A high, narrow bandpass optical filter was placed in front of the photodiode allowing the laser beam to be detected while preventing other wavelengths from reaching the photodiode. The amplified differential current signal from the quad cell photodiode, $i_{A,B,C,D}$ [$= (i_A+i_B) - (i_C+i_D) / (i_A+i_B + i_C+i_D)$], was monitored and recorded using a digital oscilloscope (TDS 780, Tektronix) or sent to a lock-in amplifier (SR850, Stanford Research Systems) for signal extraction and averaging. Photon radiation was supplied to the device with a 500°C blackbody source. The energy from the source was chopped by a mechanical chopper operating at a frequency of 1 kHz.



**Figure 3:** Schematic diagram of experimental setup.

# 3. NUMERICAL MODELING

## 3.1 Verification Model

A finite element model for the response of the device was developed through modification of a method for analyzing the effects of linear, internal strain due to thermal loads. The internal, phtoinduced strain was applied to the elements of the model using the strain relationship given in Equation 2, $\varepsilon_{pi}=1/3(dE_g/dP) \Delta n$. The pressure dependence of bandgap energy was divided by three and applied as a material property to the elements.

An external photon flux was applied to the model, and the number of charge carriers, $\Delta n$, were calculated using Equation 5. Several assumptions were made in order to perform this calculation. The quantum efficency, $\eta$, was assumed to be one. The charge carrier lifetime, $\tau_L$, was estimated to be 10 µs, and a cutoff wavelength of 7 µm was used. The charge carrier density was assumed uniform throughout the cantilever device.



Figure 4: Verification model for finite element analysis of photoinduced stress.

A verification model was created to test our method. This model consisted of a simple, rectangular cantilever beam 140 µm long by 20 µm wide, and 0.5µm thick with a 50 nm coating of Au. This beam is shown in Figure 4. One end of the beam was constrained in all six degrees of freedom and the other end was in the free condition.
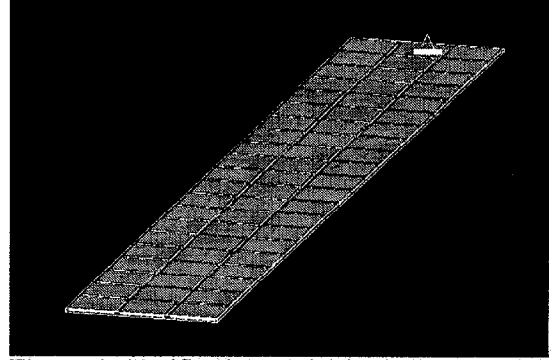
A flux of 100 µW was applied to the finite element model and the deflection results were analyzed. These results were compared with the results of Equation 4. The results of the finite element analysis predicted that the verification model would experience a displacement of 2.06 µm compared to 2.63 µm as predicted by Equation 4, a difference of 21.7%. Although closer agreement is often obtained in finite element verification models, the results were deemed sufficient enough that the finite element model could be used to estimate the mechanical response of the photoinduced effect as given by Equations 1-5.

## 3.2 Analysis of InSb Photon Detector

The FEA model of the InSb photon detector consisted of 456 two-dimensional shell elements and 456 three-dimensional solid elements. The shell elements represented a Au layer on the top surface of the device; the solid elements represented the InSb material of the cantilever. The Au layer was set to 50nm thick, and the cantilever itself was 1 µm thick. The device was 58.5 µm wide and 66 µm in height.

The dimensions of the microstructure used in the analysis were determined during fabrication. The substrate was diamond turned to a known thickness, and the thickness was further reduced using chemical etching and broad-beam ion milling. The final thickness was calculated using experimentally determined chemical etch and ion milling rates. The dimensions of the legs and pad were measured using the focused ion milling system.



Figure 5: Finite element model of InSb photon detector.

As indicated in Figure 5, the surfaces where the cantilever would be attached to an InSb substrate were constrained in all six degrees of translational and rotational freedom. The substrate that the device is attached to was not included in this analysis in order to focus on the photoinduced bending of the cantilever. The method used in Section 3.1 to analyze photoinduced stress in the rectangular beam was again applied to this more complicated microstructure. Fluxes of 1-12 µW were applied to the finite element model and the
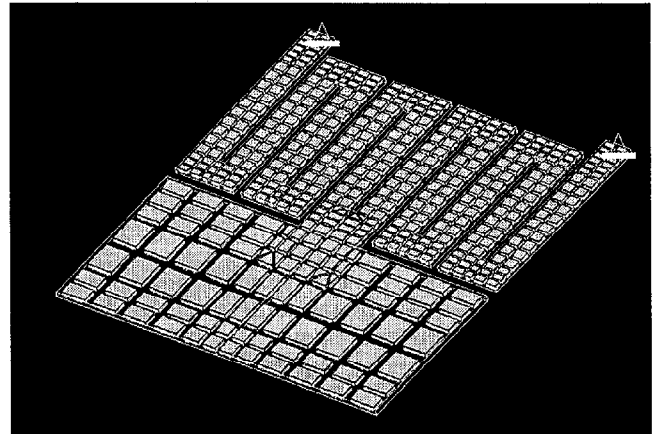
resulting deflections were computed. Convergence of all results was ensured to better than 10% using the p-element adaptive meshing technique.[26]

Modal analysis was performed on the geometry to determine the anticipated response of the structures and the mode shapes. The first four vibration modes were calculated for the InSb structure. Results of the modal analysis are used to gain insight into the potential response of the device. These results can be used to determine if a vibration mode could be excited during testing of the device.

## 4. RESULTS

The simulated photoinduced response of the cantilever to a 10 μW load is shown in Figure 6. Maximal z deflection was determined, and the z deflection was calculated at two additional points on the top surface as well: at the tip along the centerline, and in the center of the sensing pad. In all three cases, the deflection was found to vary linearly as a function of load.
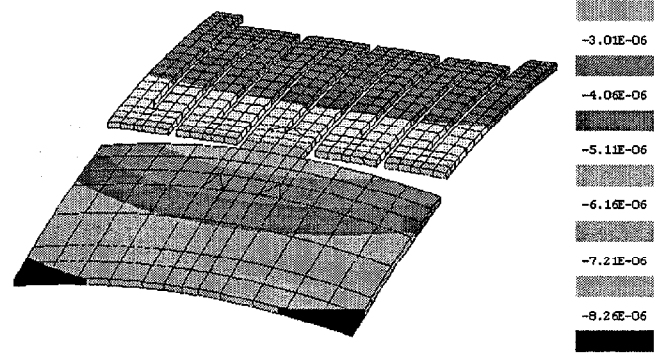
For the 10 μW flux, the maximum displacement was determined to be 9.3 nm, the tip displacement was 7.8 nm and the center displacement was 5.0 nm. Experimentally, a displacement of 25.0 nm was measured for a flux of 10.1 μW. The deflection was measured experimentally for input flux ranging from 0.7 μW to 11.3 μW. The results of the displacement simulation and experimental data are shown in Figure 7.

A modal analysis was performed to determine the first four natural vibration frequencies of the InSb folded-leg device. The mode shape for the fundamental frequency is shown in Figure 8, and the calculated frequencies for the first four vibration modes are shown in Table 1. The analysis of the mode shapes gives insight into the potential dynamic response of the device, as well as the potential motion of the device during excitation.
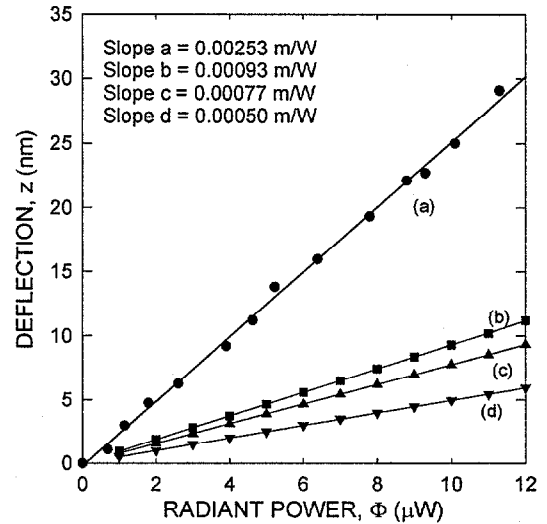
The fundamental frequency was determined to be 56.7 kHz corresponding to the normal bending vibration of the structure. The second mode was 201.44 kHz representing the twisting of the device. The third and fourth modes were more obscure vertical and side to side bending modes and occurred at 297.34 and 427.20 kHz.

## 5. DISCUSSION

A numerical method of simulating photoinduced stress was developed using the relationship for $\varepsilon_{pi}$ given in Equation 2 and using handbook values of $dE_g/dP$.[24] The $dE_g/dP$ used for InSb was $2.45 \times 10^{23}$ cm[3]. Since Au is not a semiconductor material, it was assigned a $dE_g/dP$ of zero. Radiant power was applied to the model ranging from 1 to 12 μW. The radiant power was used to determine the elemental value of $\Delta n$. The value of $\Delta n$ in the volume of the sensor was determined by the relationship given in Equation 5, and assuming a quantum efficiency of one, a charge carrier lifetime of 10 μs, and an incident wavelength of 7 μm.
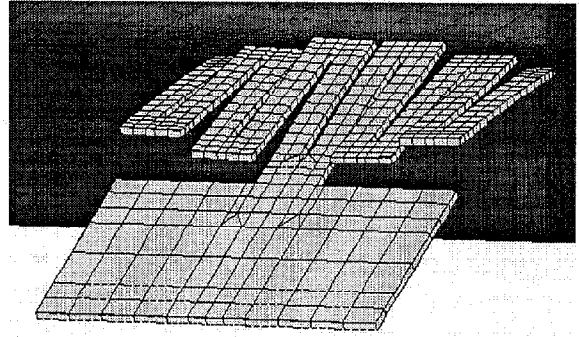
**Figure 6:** Simulated photo-induced bending of InSb microstructure from the 10 μW flux. The deformed shape of the structure is exaggerated. The scale on the right is in units of mm.

**Figure 7:** Plot of (a) experimental data and (b-d) modeling data for three points giving deflection as a function of radiant power. (a) Average experimental deflection, (b) maximum z deflection, (c) tip deflection, and (d) deflection near the center of the sensing pad.

**Table 1:** InSb microstructure frequencies of vibration

| Mode | Frequency (kHz) |
|------|-----------------|
| 1 | 56.66 |
| 2 | 201.44 |
| 3 | 297.34 |
| 4 | 427.20 |



**Figure 8:** Fundamental mode of vibration

A verification analysis was performed using the numerical method for simulating photoinduced stress. The results of the verification model were compared with the results of Equation 4. The results of the verification model showed agreement within 22% with the results from Equation 4. While the results were in close enough agreement to indicate that the analysis technique is useful in understanding the phenomenon of photoinduced stress, we were concerned that closer correlation was not achieved for the simple geometry. The relation for strain in both instances was based on the linear expression for strain given in Equation 2. The disagreement of these two methods indicates that discrepancies are present in the basic assumptions made both for calculating the deflection and for creating the finite element model. Further investigation of these discrepancies is necessary. The references for Equation 2 were unclear whether Equation 2 is an exact solution or an approximation.

Figure 6 displays the exaggerated deformed structure due to photoinduced bending. The curvature of the sensing pad is due to the isotropic photoinduced expansion of the InSb structure combined with the constriction of the InSb layer by the Au coating. The results of the experimental measurement of the device are plotted with the modeling data in Figure 7. The experimental values for the maximum z deflection were 2.5 times greater than those predicted by the model. Others[27] have experienced higher experimental photoinduced deflections than predicted by their models.

Several sources of error are possible in the model. One of the most difficult terms to measure to a high accuracy is the thickness of the sample. Because the thickness of the sample affects both the charge carrier density and the moment of inertia of the structure, the amount of bending in the sample is a function of the thickness to the fourth power. It was determined that a twenty-percent error in determining the thickness of the sample would result in a factor of two error in the calculated deflection. Also, the finite element model assumed that no effects other than photoinduced bending were present and that the distribution of charge carriers was uniform in the in the volume. A higher distribution of charge carriers on the surface of the material would add to the bimaterial effect and could result in an increased amount of deflection. The assumption that $3Y = c_{11} + 2c_{12}$ used to obtain Equation 2 is valid to better than two percent in the case of InSb and was not deemed a source of error.

Figure 8 shows the deformed geometry from the vibration analysis, which corresponds to the normal vertical bending of the device. The second mode of vibration corresponded to a twisting of the device. The third and fourth modes corresponded to more obscure bending of the legs and side to side bending modes, however the separation of the modes made it unlikely that the higher modes would be excited. The energy input to the device was chopped at a frequency of 1 kHz, making it unlikely that the resonance frequency of the structure was excited during testing.

## 6. CONCLUSIONS

Finite element analysis has proven to be a very useful tool in designing microstructures and understanding their behavior. Simple changes in the geometry of micro-sensors can have significant effects on their response. In this experiment, a finite element model for the electronic bending of semiconductor structures was developed based on previously formulated relationships. The model was shown to have coarse agreement with the previously derived relationships. Better agreement

was expected with the structural relationships, and it may be necessary to look at the derivation of the relationships. Experimental results were 2.5 times higher than those predicted by the model. The high experimental results speak of the promise of the use of InSb as a micromechanical photon detector. Differences in the results of the finite element model and the experimental data are likely due to difficulties in quantifying the geometric data.

## ACKNOWLEDGEMENTS

## REFERENCES

1.  R.J. Kayes, *Optical and Infrared Detectors*, Vol. 19. Berlin: Springer-Verlag, 1977.
2.  J. L. Miller, *Principles of Infrared Technology*, Van Nostram Reinhold, New York, 1994.
3.  E. L. Dereniak and G. D. Boreman, *Infrared Detectors and Systems* Wiley and Sons, New York, 1996.
4.  A. Rogalski, "New Trends in Infrared Detector Technology," *Infrared Phys. Technol.* **35**, 1, 1994.
5.  C. Hanson, "Uncooled Thermal Imaging at Texas Instruments," Infrared Technology XXI, SPIE **2020**, 330, 1993.
6.  R. A. Wood and N. A. Foss, "Micromechanical Bolometer Arrays Achieve Low-Cost Imaging," Laser Focus World, 101, June, 1993.
7.  P.W. Kruse, "Uncooled IR Focal Plane Arrays," *Infrared Technology XXI*, SPIE **2552**, 556, 1995.
8.  P.G.Datskos, P.I. Oden, T. Thundat, E.A. Wachter, R.J. Warmack, and S.R. Hunter, "Remote Infrared Detection Using Piezoresistive Microcantilevers," *Appl. Phys. Lett.* **69**, 2986, 1996.
9.  P.G. Datskos, S. Rajic, I. Datskou, and C.M. Egert, "Novel Photon Detection Based on Electronically-Induced Stress in Silicon," SPIE **3779**, pp. 173-181, 1998.
10. P.G. Datskos, S. Rajic, and I. Datskou, "Photoinduced and thermal stress in silicon microcantilevers," *App. Phys.Lett.* **73**, (16) pp. 173-181, 1998.
11. P.G. Datskos, S. Rajic, I. Datskou, and C.M. Egert, "Detection of Infrared Photons Using Electronic Stress in Metal-Semiconductor Interfaces," *Ultramicroscopy*, (in press).
12. P.G. Datskos, S. Rajic, I.Datskou, and C.M. Egert, "Infrared Microcalorimetric Spectroscopy Using Uncooled Thermal Detectors," *SPIE Vol. 3118*, pp 280-287, 1997.
13. P.G. Datskos and I. Sauers, "Detection of 2-Mercaptoethanol Using Gold Coated Micromachined Cantilevers," *Sensors and Actuators B – Chemical,* (in press).
14. R.G. Stearns and G.S. Kino, "Effect of electronic strain on photoacoustic generation in silicon," *Appl. Phys. Lett.* **47** (10) pp. 1048-1050, 1985.
15. D.M. Todorovic, P.M. Nikolic, and A.I. Bojicic, "Photoacoustic frequency transmission technique: Electronic deformation mechanism in semiconductors," *J. Appl. Phys.* **85** (11) pp. 7716-7726, (1999).
16. T. Figielski,, "Photostriction Effect in Germanium," *Phys. Status Solidi 1*, **306**, 1961.
17. G.R. Buchanon, *Mechanics of Materials*, Holt, Reinhart, and Winston, Inc. New York, 1988.
18. A. Prak and T.S.J. Lammerink., "Effect of Electronic Strain on the Optically Induced Micanical Moment in Silicon Microstructures," *J. Appl. Phos.* **71** (10), pp. 5242-5245 1992.
19. P.J. Shaver, "Bimetal Strip Hydrogen Gas Detectors," *Rev. Sci. Inst.*, **40** (7), pp. 901-905, 1969.
20. E.A. Wachter, T. Thundat, P.I.Oden, and R.J. Warmack, "Remote optical detection using microcantilevers," *Rev. Sci Instrum.* **67** (10), pp. 3434-3439, 1996.
21. O.C. Zienkiewicz, *The Finite Element Method in Structural and Continuum Mechanics,* McGraw-Hill, London, 1967.
22. J.E. Akin, *Finite Elements for Analysis and Design,* Academic Press Limited, San Diego, 1994.
23. A.J. Baker and D.W. Pepper, *Finite Elements 1-2-3,* McGraw-Hill, Inc. 1991.
24. Weast, R.C., *CRC Handbook of Chemistry and Physics*, CRC Press, Inc. Boca Raton, Fl, 1988.
25. P. Klocek, *Handbook of Infrared Optical Materials*, Marcel Dekker, Inc. New York, 1991.
26. B.M. Evans III, P. Datskos, S. Rajic, and I. Datskou, "Optimization of Micromachined Photon Devices," *SPIE*, **3778**, 1999.
27. J.R. Buschert and R. Colella, "Photostriction Effect in Silicon Observed by Time Resolved X-Ray Diffraction," *Sol. State. Comm.*, **80**, (6), pp. 419-422, 1991.